J Mater Sci (2009) 44:3841–3851
DOI 10.1007/s10853-009-3521-9

Constitutive models of creep for lead-free solders

Hongtao Ma

Received: 30 December 2008 / Accepted: 25 April 2009 / Published online: 15 May 2009

Abstract The constitutive modeling of creep has been extensively studied due to the important of the creep failure mode in solder joints. However, there are very few studies that considered room temperature aging contributions in their creep modeling studies. This study investigated constitutive modeling of creep of solders by taking into account the possible contribution room temperature aging. Lead-free solder (Sn–4.0Ag–0.5Cu) was found to have a higher creep resistance than Sn–Pb solder at the same stress level and testing temperature. The higher creep resistance was contributed by the second phase intermetallic compounds, Ag_3Sn and Cu_6Sn_5. The precipitation of these intermetallic compounds can significantly block the movement of dislocations and increase the creep resistance of the material. Constitutive models of creep for both lead-free and Sn–Pb eutectic solders were constructed based on the experimental data. The activation energy for SAC405 is much higher than that of Sn–Pb, which also indicates that SAC405 possesses higher creep resistance. The constitutive models can be used in finite element analysis of actual electronic packages to predict solder joint failure. The creep mechanisms of both lead-free and Sn–Pb eutectic solders were also extensively discussed in this dissertation. Dislocation gliding and climb is believed to be the major failure mode at high stresses, while lattice diffusion and grain boundary diffusion is believed to be the major failure mode at low stress levels. Grain boundary sliding is believed to contribute to creep deformation at both high-stresses and low-stresses. For eutectic Sn–Pb, superplastic deformation is a major the creep mechanism at low-stresses and high-temperatures.

H. Ma (✉)
Auburn University, 36849 Auburn, AL, USA
e-mail: hongtaoma@hotmail.com

Introduction

Solder joints in electronic packaging components are very complex elements. The study of solder joint reliability is also complex, especially in determining the mechanical reliability. Creep deformation is the dominant deformation in solder joints due to their high homologous temperatures. Creep analysis is often adopted as one of the major approaches used to predict the end-of-life for solder joints by finite element analysis. Creep analysis of lead-free solders has been heavily studied. However, there are large discrepancies in current data.

Creep generally refers to the time-dependent strain plastic deformations at constant uniaxial stress [1–3]. Creep deformation tends to be rapid when the homologous temperature is above 0.5 T_m. Figure 1, shows a typical creep curve for lead-free solders, which generally consists of three stages after the initial instantaneous strain when a constant load is applied [1]. However, the secondary, or steady-state creep is the dominant deformation experienced by solder alloys. In this stage, the strain rate is retarded by strain-hardening, which decreases the deformation speed, while the associated recovery and recrystallization (softening) tend to accelerate the creep rate [2]. The steady-state creep rate can be quantitatively estimated, and a series of constitutive models have been proposed. The following two models are the most widely accepted for the characterization of solder alloys by considering the diffusion controlled creep deformation mechanism.Dorn Power Law [4]:

$$\dot{\varepsilon} = A\sigma^n \exp\left(-\frac{Q}{RT}\right) \tag{1}$$

Garofalo Hyperbolic Sine Law [2]:

$$\dot{\varepsilon} = C[\sinh(\alpha\sigma)]^n e^{\left(\frac{-Q}{RT}\right)} \tag{2}$$

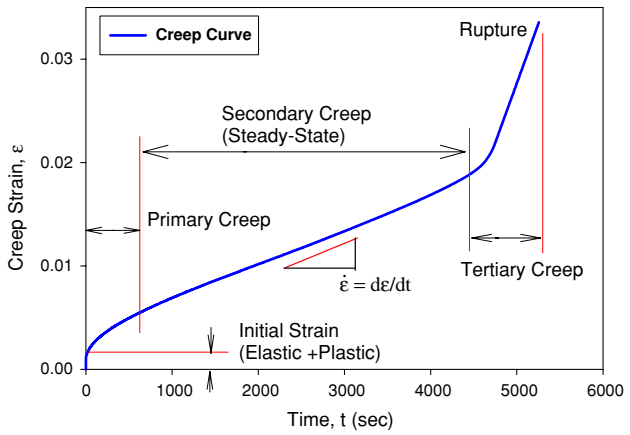

Fig. 1 Typical creep curve for lead-free solders

where R is the universal gas constant, T is the temperature in Kelvin, σ is the applied stress, A and C are material dependent constants, n is the stress exponent, and Q is the activity energy. The models show that the steady state creep strain rates are strongly stress and temperature dependent.

Constitutive modeling of creep deformation has been a heavily studied and researched area due to the importance of being able to predict the end of life of electronic packaging using finite element analysis tools. Many models have been proposed and modified by researchers. As previously mentioned, the Dorn power-law and Garofalo Hyperbolic models are the most widely accepted models for solder alloys. The constitutive model can be determined by creep testing at different temperature and stress levels. Tables 1 and 2 summarize some of the current data for both near eutectic Sn–Ag–Cu ((Sn–(3.0–4.0)Ag–(0.5–1.0)Cu)) lead-free solder alloys and Sn–Pb; all the models are based on steady-state creep. Materials constants, specimens, and testing methods are compared in the tables. The majority of the data can be fitted into the Hyperbolic Sine model. As with the testing of tensile properties, there are large discrepancies in the creep data and materials constants vary over a very large range. The materials constants are important in determining the accuracy of end-of-life prediction for solder joints using finite element analysis. Large discrepancies would degrade the accuracy of these predictions.

Figure 2 summarizes several of the hyperbolic sine models for near eutectic Sn–Ag–Cu (Sn–(3.0–4.0)Ag–(0.5–1.0)Cu) alloys at 125 °C, showing how the steady-state creep rate varies over a very large range. Clech [5] reviewed creep modeling for both Sn–Pb and lead-free solder alloys based on the currently available data under an NIST project, and commented that the current database are widely scattered. Discrepancies may be caused by differences in the specimen, testing method, and testing conditions. However, none of the previously documented data has recognized the possible effects of room temperature aging on creep deformation, which may be one of the major reasons causing these the data discrepancies [6, 7].

Creep modeling studies have also been investigated for other lead-free solders. Mitlin et al. [8, 9] have found that steady-state creep of Sn–Bi solders also closely follows

Table 1 Garofalo hyperbolic creep models of solder alloys

Constitutive models	Solder alloy	Constants				Specimen testing method	Reference sources
Garofalo hyperbolic sine law		C	α (MPa^{-1})	n	Q (kJ/mol)		
$\dot{\varepsilon} = C[\sinh(\alpha\sigma)]^n e^{\left(\frac{-Q}{RT}\right)}$	Sn–40Pb	0.1114	751	3.3	53.0	Lap-joints, shear/tensile	Darveaux [20]
	Sn–37Pb	0.158	0.406	1.38	50.0	Cast bulk, tensile	Xiao [21]
		10.0	0.1	2	44.9	Flip chip joints, tensile	Wiese [22]
		2.87×10^{-5}	1300	3.3	52.8		Shi [23]
		1999.4	0.2	2.1	54.1	Lap-joint, tensile	Zhang [24]
	Sn–3.5Ag	178.5	0.115	4.75	57.1	Bulk, tensile	Wiese [22]
		23.17	0.0509	5.04	41.6	Bulk, tensile	Clech [5]
		8.18×10^{11}	0.0266	8.67	77.4	Lap joint, shear	Clech [5]
		2.46×10^{5}	0.0913	5.5	72.5	Lap joint, shear	Clech/Darveaux [5, 25]
	Sn–3.0Ag–0.5Cu	2631	0.0453	5.0	52.4		Vianco [26]
	Sn–3.9Ag–0.6Cu	0.184	0.221	2.89	62.0	Cast bulk, tensile	Xiao [21]
		4.41×10^{5}	0.005	4.2	45	Bulk, compression	Lau and Vianco [27]
		3.49×10^{4}	0.005	4.3	43.13	Bulk, compression	Vianco [28]
		248.4	0.188	3.79	62.3	Lap-joint, tensile	Zhang [24]
	Sn–3.8Ag–0.7Cu	3.2×10^{4}	0.037	5.1	65.3	Bulk, tensile	Pang [29]
		2.78×10^{5}	0.0245	6.41	54.2		Schubert [30]
	SAC series	7.93×10^{5}	0.0356	5	67.9	Fitting data	Clech [5]

Table 2 Dorn power-law creep models of solder alloys

Constitutive models	Solder alloy	Constants			Specimen testing method	Reference sources
Dorn power law		A (s^{-1})	n	Q		
$\dot{\varepsilon} = A\sigma^n \exp\left(-\frac{Q}{RT}\right)$	Sn–3.5Ag	5×10^{-6}	11	79.8	Flip chip, tensile	Wiese [22]
		9.44×10^{-5}	6.05	61.1	Bulk, tensile	Clech [5]
	Sn–4.0Ag–0.5Cu	2×10^{-21}	18	83.1	Flip chip, tensile	Wiese [22]

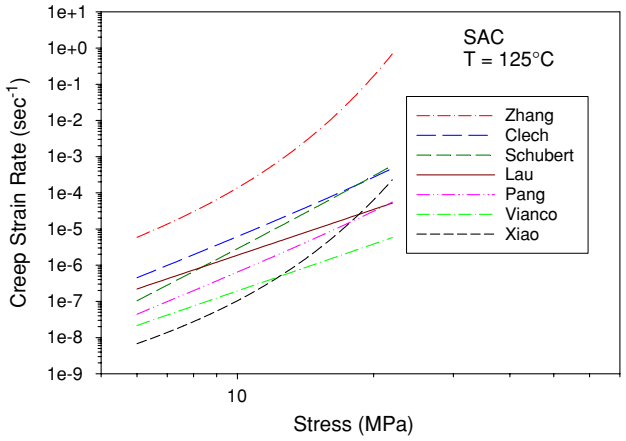

Fig. 2 Discrepancies in the creep models

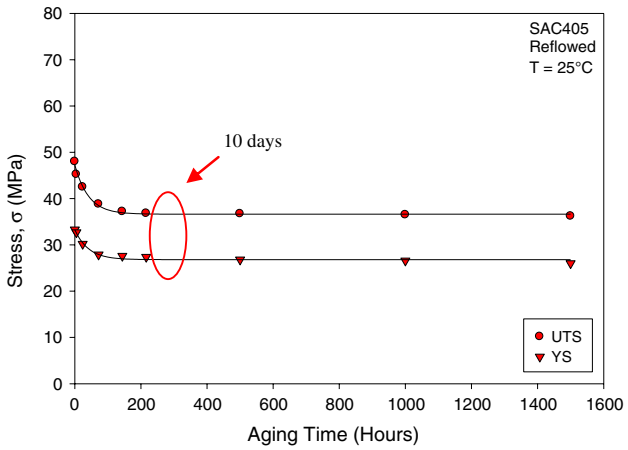

Fig. 3 Stress degrading during room temperature aging [6]

hyperbolic sine relation, and higher Bi content appears with higher creep resistance. El-Rehim et al. [10] found that increasing of grain size increases the creep resistance of Sn–Bi lead-free solders, the results may be helpful to understand the evolution of creep performance with the evolution of microstructure. Recent researches also explore the effects of micro addition effects on creep performance of lead-free solders, Cheng et al. [11] found that addition of Co or Ni will improve the ductility of Sn–3.0Ag–0.5Cu (SAC305) solder alloy. Pang and co-workers studied the addition of Ce in SAC305, which improves the general tensile strength of SAC alloys, however, the creep results shows Ce addition improves creep at higher stress level, but has worse creep performance at lower stress level [12, 13]. The creep variation is believed to relate to additional IMC formations. Their results also show hyperbolic sine model fits lead-free creep better than that of power law model.

The recent results shows that room temperature aging effects will dramatically affect the mechanical properties of solder alloys [6, 7]. Any difference in the testing conditions of specimens could seriously affect the accuracy of the data. The data shows that the tensile strength significantly degrades during room temperature aging up to 2 months of aging time by up to 35%. The creep resistance also degrades at room temperature. The data also shows that the tensile properties of SAC405 (Sn–4.0Ag–0.5Cu) lead-free solders after 10 days of aging at room temperature (as shown in Fig. 3) tend to be relatively stable.

In this study on creep modeling, in order to reduce the effects of room temperature aging effects, reflowed specimens were aged at room temperature for 10 days before testing to reduce the contribution of decreasing creep resistance at room temperature. All specimens were tested under the same testing conditions. Steady-state creep strain rates were obtained and data fitted with the available constitutive models in this study.

Experimental procedure

The solder specimens are originally formed in rectangular cross-section glass tubes using a vacuum suction process. The solder is first melted in a quartz crucible using a pair of circular heating elements (illustrated in Fig. 4). A thermocouple attached on the crucible and a temperature control module is used to direct the melting process. One end of the glass tube is inserted into the molten solder, and suction is applied to the other end via a rubber tube connected to the house vacuum system. The suction forces are controlled through a regulator on the vacuum line so that only a desired amount of solder is drawn into the tube. The

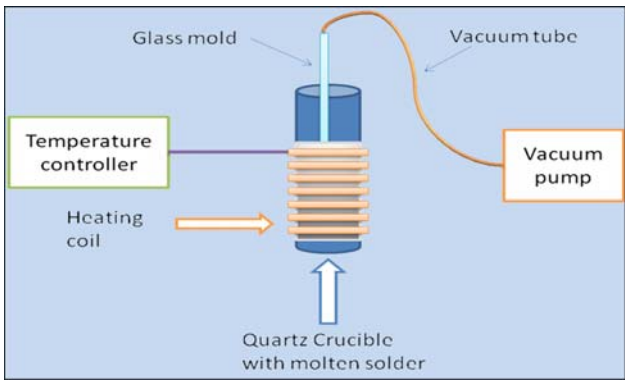

Fig. 4 Illustration of specimen preparation setup

specimens are then cooled to room temperature using a user-selected cooling profile.

In order to see the extreme variations possible in the mechanical behavior and microstructure, we are exploring a large spectrum of cooling rates including water quenching of the tubes (fast cooling rate), air cooling with natural and forced convection (slow cooling rates), and controlled cooling using a surface mount technology solder reflow oven. Typical temperature versus time plots for water quenching and air cooling of the test samples are shown in Fig. 5. For the reflow oven controlled cooling, the solder in the tubes is first cooled by water quenching, and then sent through a reflow oven (9 zone Heller 1800EXL) to remelt the solder in the tubes and subject them to the desired temperature profile. Thermocouples are attached the glass tubes and monitored continuously using a radio-frequency KIC temperature profiling system to ensure that the samples are formed using the desired temperature profile (same as actual solder joints). Figure 6 illustrates the reflow temperature profiles used in this work for Sn–4.0Ag–0.5Cu (SAC405) and Sn–37Pb (SnPb) solder specimens.

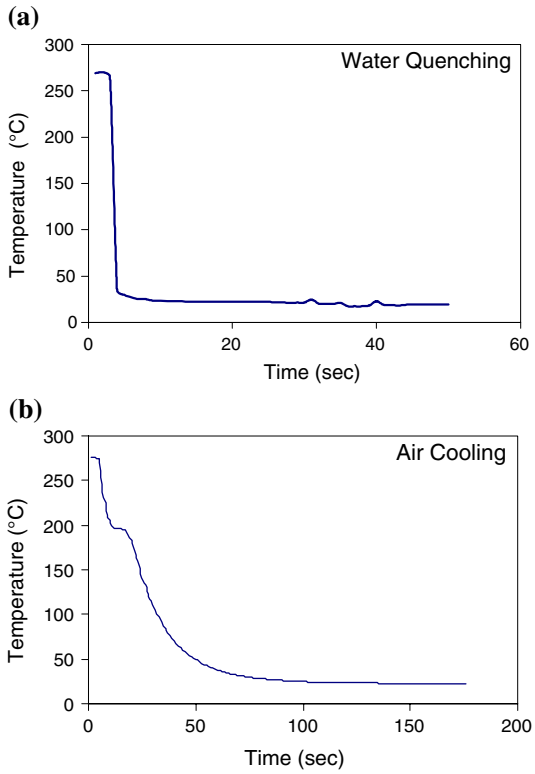

Fig. 5 Sample cooling profiles. **a** Water quenched, **b** air cooled

Typical glass tube assemblies filled with solder and a final extracted specimen are shown in Fig. 7. For some cooling rates and solder alloys, the final solidified solder samples can be easily pulled from the tubes due to the differential expansions that occur when cooling the low CTE glass tube and higher CTE solder alloy. Other options for more destructive sample removal involve the breaking of the glass. The final test specimen dimensions are governed by the useable length of the tube that can be filled with solder, and the cross-sectional dimensions of the hole running the length of the tube. In this work, we formed uniaxial samples with nominal dimensions of 80 × 3 × 0.5 mm. A thickness of 0.5-mm was chosen because it matches the height of typical BGA solder balls. The described sample preparation procedure yielded repeatable samples with controlled cooling profile (i.e., microstructure), oxide free surface, and uniform dimensions. By extensively cross-sectioning of several specimens, we have verified that the microstructure of any given sample is consistent throughout the volume of the sample. In addition, we have established that our method of specimen preparation yields repeatable sample microstructures for a given solidification temperature profile. Samples were inspected using a micro-focus X-ray system to detect flaws (e.g., notches and external indentations) and/or internal voids (non-visible).

A tension/torsion thermo-mechanical test system has been used to test the samples in this study. The system provides an axial displacement resolution of 0.1 μm and a rotation resolution of 0.001°. Testing can be performed in tension, shear, torsion, bending, and in combinations of these loadings, on small specimens such as thin films, solder joints, gold wire, fibers, etc. Cyclic (fatigue) testing can also be performed at frequencies up to 5 Hz. In addition, a universal 6-axis load cell was utilized to simultaneously monitor three forces and three moments/torques during sample mounting and testing. Environmental chambers added to the system allow samples to be tested over a temperature range from approximately −185 to +300 °C.

Using specimens fabricated with the casting procedure described above, creep behavior has been characterized for SAC405 and SnPb lead-free solders. In creep experiments, constant stress levels on the order of 40–50% of the

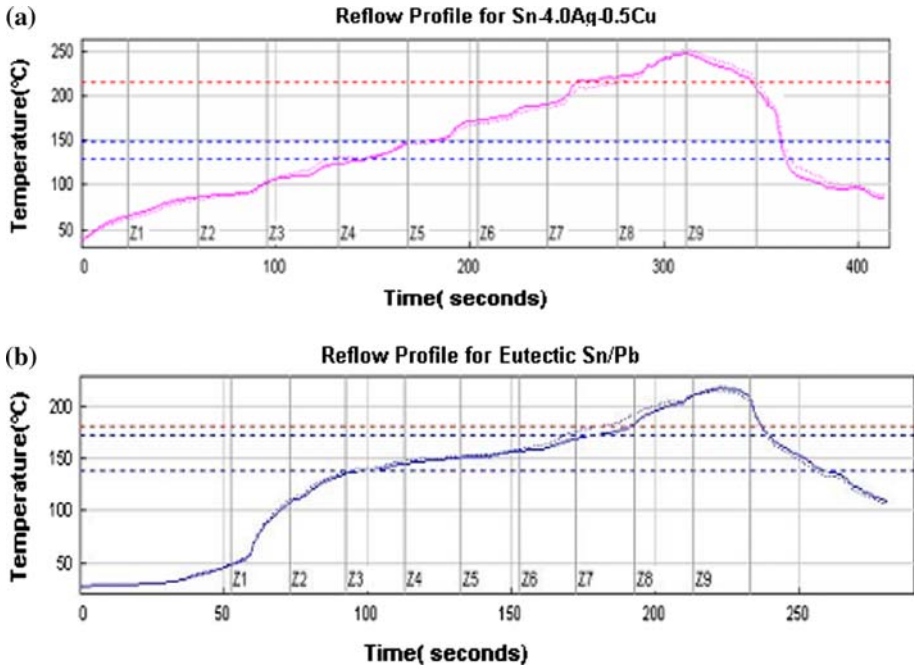

Fig. 6 Solder reflow temperature profiles. **a** SAC405, **b** Sn–Pb

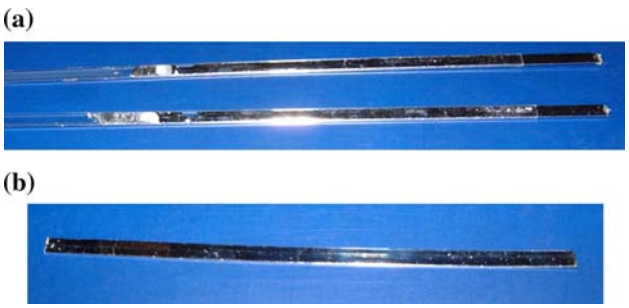

Fig. 7 Solder uniaxial test specimens. **a** Within glass tubes, **b** after extraction

observed UTS were applied. In this study, tests using various applied stresses at different temperatures were performed. The strain versus time responses were recorded and the "steady state" creep strain rates (creep compliance) in the secondary creep region were evaluated. In this study, the "steady state" secondary creep rate was defined to be the minimum slope value of the observed $\dot{\varepsilon}$ versus t response in the secondary creep region.

The lead-free solder test results presented in this study were all for samples solidified with the reflowed (Fig. 6a) cooling profile (mimics that seen by actual solder joints during PCB assembly). Finally, in all of the lead-free (SAC) testing performed, analogous experiments were also performed with reflowed 63Sn–37Pb eutectic solder samples for comparison purposes.

Results and discussion

Constitutive relationship for lead-free and Sn–Pb eutectic solders

Creep testing was carried out at different stress levels and various temperatures. Four stress levels were chosen, 20, 15, 10, and 7 MPa for both reflowed SAC405 and Sn–Pb specimens. Testing was completed at five temperature levels, 25, 75, 100, 125 and 150 °C. All tests were conducted using the Micro-tester with the thermal chamber attached. Figure 8 illustrates a typical set of creep curves at different stress levels for SAC405 solder. The creep deformation increases with increasing stress levels. Higher stresses will accelerate the movement of dislocations, which includes dislocation gliding and climb. Higher stresses will also induce greater grain boundary gliding. Dislocation gliding and grain boundary sliding are the major creep mechanisms for creep deformation. Figure 9 shows a set of typical creep curves at various temperatures and the same stress level, indicating that higher temperatures induces more severe creep deformation in solder alloys. Creep deformation is diffusion controlled, so a higher temperature will lead to a higher diffusion rate and a higher creep rate. Figure 10 summarizes the steady-state creep strain rates versus stress levels at various temperatures. The experimental data were fitted by multiple variables data fitting according to both the Garofalo Hyperbolic

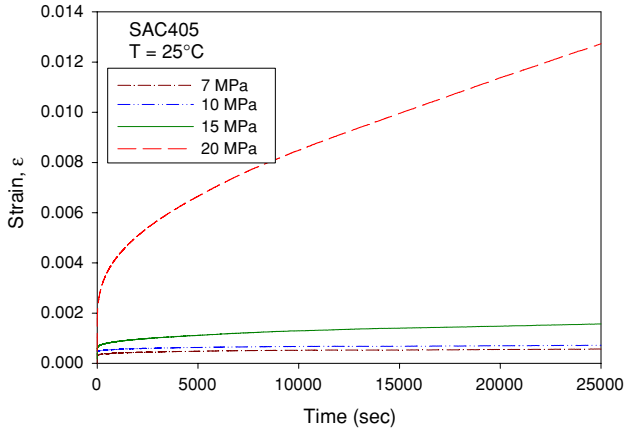

Fig. 8 SAC405 creep curves at different stress levels

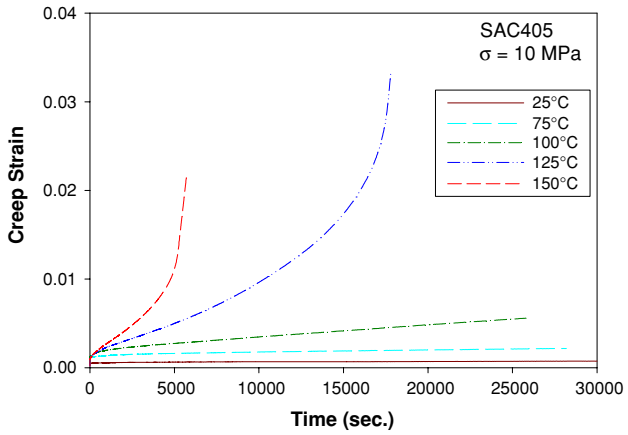

Fig. 9 SAC 405 creep curves at different testing temperatures

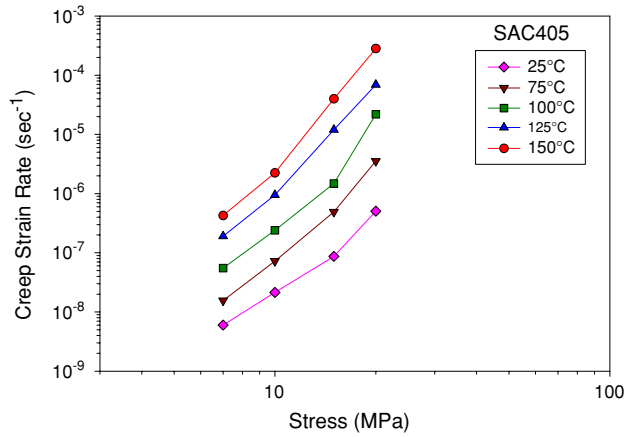

Fig. 10 Experimental results of SAC405 steady-state creep strain rate

Sine Law and the Dorn power-law. Figure 11 shows the hyperbolic fitting of the experimental data, and Fig. 12 illustrates the power-law fitting to the same experimental data.

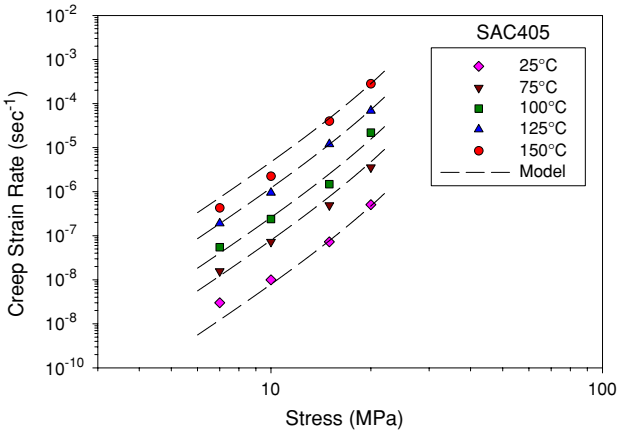

Fig. 11 Hyperbolic sine creep model of steady-state creep strain rate of SAC405

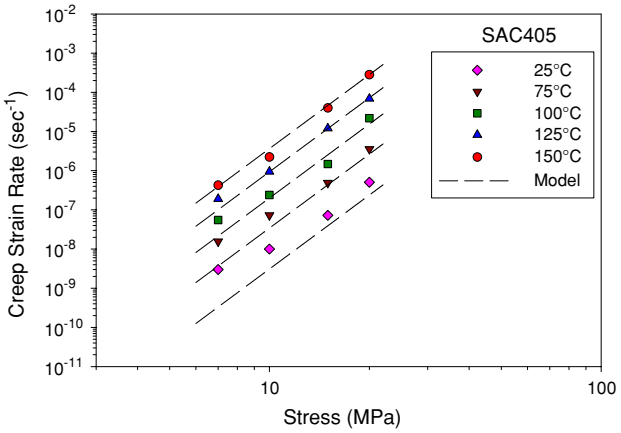

Fig. 12 The power-law model of steady-state creep strain rate of SAC405

All the materials constants were obtained by multiple variable data fitting methods. Equation 3 is the hyperbolic sine law fitting of the SAC405 creep model. Equation 4 is the fitting for the power-law model. Figure 13 compares the two models at the same testing temperature and stress level for the SAC405 alloy. The results indicate that at higher stress levels above 15 MPa, both models have an almost identical fit to the experimental data. However, at lower stress levels, hyperbolic sine model fits the experimental data better than the power-law model. The obtained constitutive models can be used to predict the end-of-life of the solder joints in numerical techniques such as finite element methods. Overall, Garofalo's hyperbolic model is a better model to fit the current experimental data. Figure 14 illustrates the comparison of the new constitutive model for SAC solder alloy with the models proposed by other researches (Table 1 and Fig. 2), indicating that the

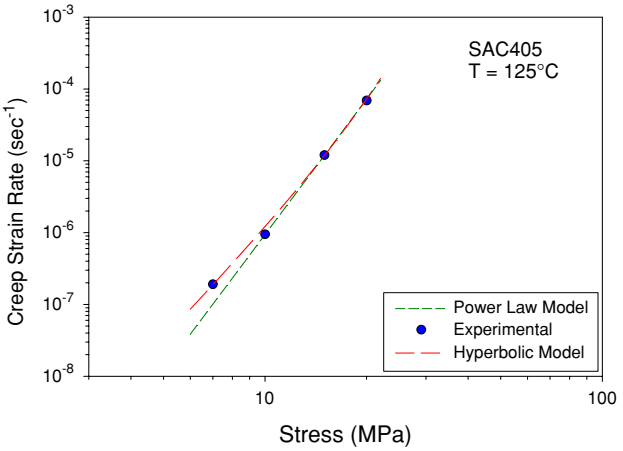

Fig. 13 Comparison of hyperbolic sine model and power-law model (SAC405)

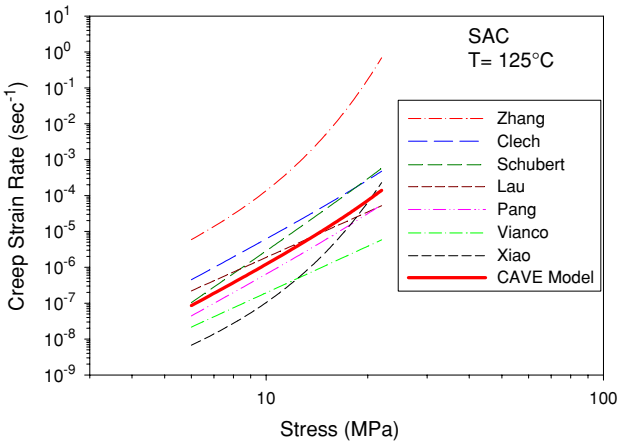

Fig. 14 Comparison of constitutive creep models of sac solder alloys

new model appears to lie in the middle of all the current models for SAC alloys. As previously mentioned, there are large discrepancies in the current data on constitutive modeling of creep. The discrepancies and data scattering may be caused by many factors, such as specimen preparation and cooling rate, specimen geometry and size, and testing conditions and testing methods. However, none of the currently documented data have recognized the possible contribution of room temperature aging effects in their studies of creep deformation analysis. Room temperature aging effects may be one of the major factors that are causing the large discrepancies in the current data.

$$\dot{\varepsilon} = 1.77E+05[\sinh(5.48E-02\sigma)]^{4.89}\exp\left(-\frac{76.13}{RT}\right) \quad (3)$$

$$\dot{\varepsilon} = 5.09E-03\sigma^{6.27}\exp\left(-\frac{76.2}{RT}\right) \quad (4)$$

Corresponding data were also collected for reflowed Sn–Pb eutectic solder alloy and are illustrated in Figs. 15, 16, 17, 18, 19, and 20. The figures reveal a similar trend

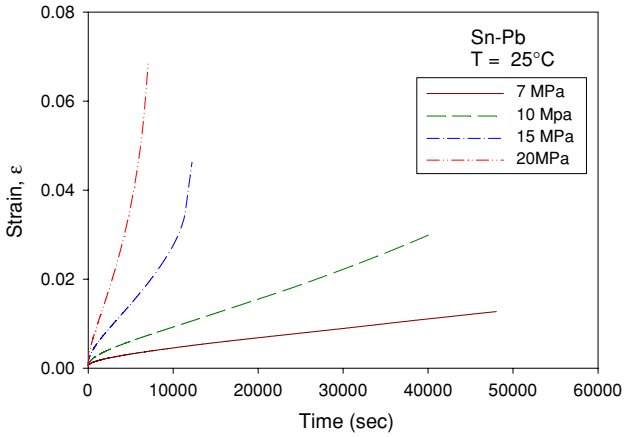

Fig. 15 Sn–Pb creep curves at different stress levels

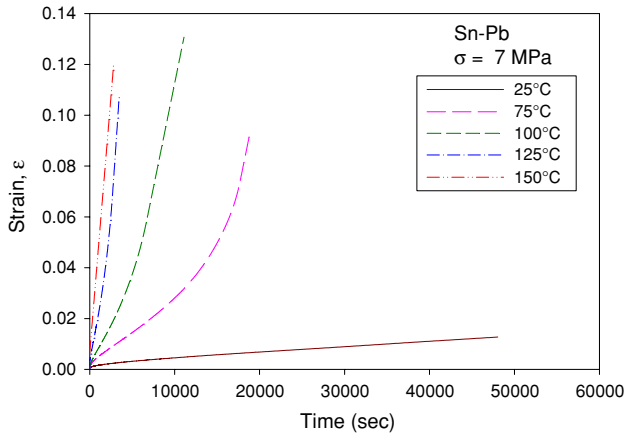

Fig. 16 Sn–Pb creep curves at different testing temperatures

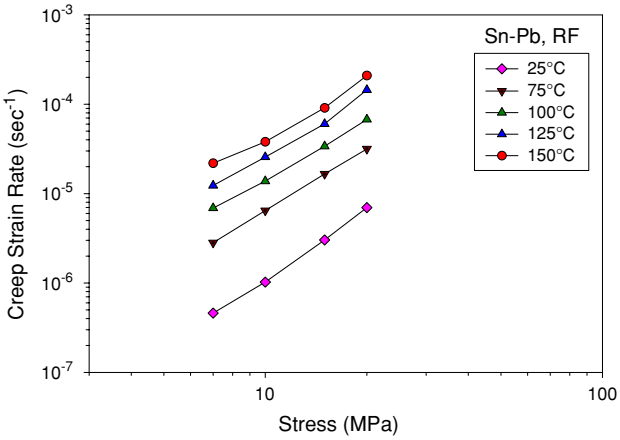

Fig. 17 Sn–Pb steady-state creep strain rate versus stresses

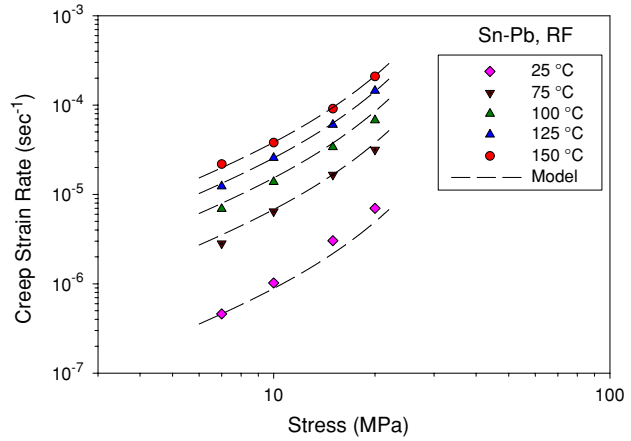

Fig. 18 Hyperbolic sine creep model of Sn–Pb steady-state creep strain rate

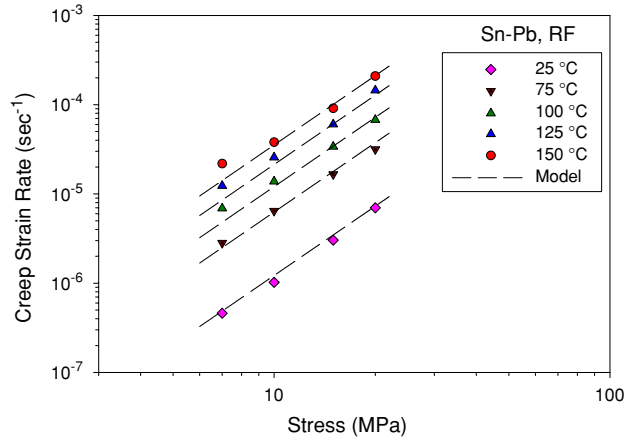

Fig. 19 The power-law model of steady-state creep strain rate for Sn–Pb

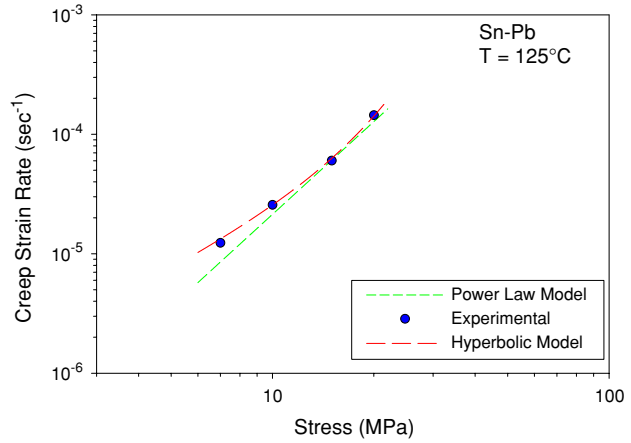

Fig. 20 Comparison of constitutive creep models (Sn–Pb)

as that of SAC405, where the higher stress and higher temperature induced more severe creep deformation (Figs. 15, 16).

The collected experimental data (Fig. 17) were also fitted with multiple variables data fitting for both the Garofalo Hyperbolic Sine Law and the Dorn power-law models. The hyperbolic sine model for Sn–Pb is shown in Eq. 5, and the power-law model is shown in Eq. 6. Figure 20 shows the comparison between the two models for Sn–Pb eutectic solder alloy, and indicates similar results to those for SAC405. The two models show similar perfect fitting at higher stress levels above 15 MPa, and once again, the hyperbolic sine law model exhibits a better fit at lower stress levels. Overall, the Garofalo Hyperbolic Sine Law provides a better fit for the experimental data for Sn–Pb.

$$\dot{\varepsilon} = 0.908[\sinh(0.105\sigma)]^{1.51}\exp\left(-\frac{35.74}{RT}\right) \tag{5}$$

$$\dot{\varepsilon} = 2.87E-04\sigma^{2.58}\exp\left(-\frac{33.30}{RT}\right) \tag{6}$$

Comparing to the materials constants of Sn–Pb (Eq. 5, 6) with that of SAC405 (Eq. 3, 4), the activation energy of Sn–Pb is significantly smaller than that of the SAC405 alloy, indicating that the creep resistance of SAC405 is higher than that of the Sn–Pb. The stress component of Sn–Pb is also significantly smaller than that of SAC405, which also indicates lower creep resistance for Sn–Pb.

Comparing Sn–Pb and SAC405, SAC405 has a higher creep resistance than Sn–Pb at the same stress level and testing temperature (Fig. 21). The constitutive models also show that the SAC alloy possesses higher activation energy than Sn–Pb, which indicates that the SAC alloy has a higher creep resistance than Sn–Pb. Activation energy represents the height of the energy barrier the atoms have to overcome to diffuse and move to lower energy levels (as shown in Fig. 22). Dorn, Garofalo and Weertman independently found that the creep activation energy equals the self-diffusion activation energy when $T_h \geq 0.5T_m$ [1, 2, 14,

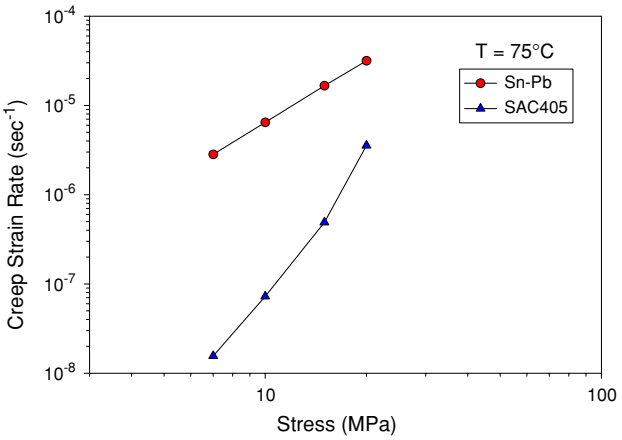

Fig. 21 Comparison of creep rate of Sn–Pb versus SAC405

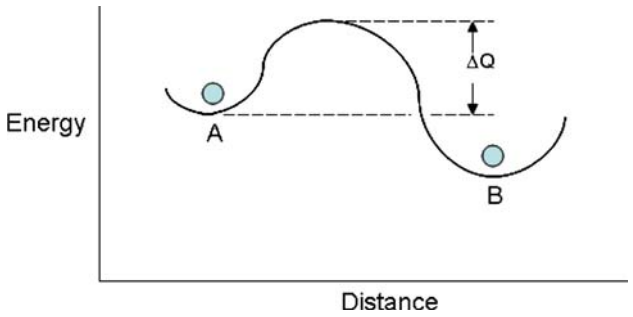

Fig. 22 Activation energy required for atomic diffusion

15]. The homologous temperatures in the operational temperature range of solder alloys are greater than half of the melting points, indicating that the self-diffusion activation energy is the barrier that atoms must overcome to cause creep deformation in solder alloys, which corresponding to their levels of creep resistance.

The stress component in creep models represents the contribution of the applied stress effects to creep deformation. The values of these stress components are spread over a very large range. Hanke et al. [16] proposed that the steady-state creep rate can be categorized in four regions. As illustrated in Fig. 23, regions I and II are grain or phase size dependent which possess low-stress component ranges from 1 to 3. Region III and IV are independent of grain or phase size, and have higher stress components ranging from 3 to above 10. Schubert et al. [17] concluded that the steady-state creep rate for lead-free solders fit into region III and IV, and thus can be predicted by Garofalo Hyperbolic Sine Model. Grivas et al. studied the Sn–Pb solder creep phenomena [18], and found that the steady-state creep model for Sn–Pb lies in region II and III. The differences of creep phenomena between lead-free and Sn–Pb solders are very apparent. In this study, the stress component n is 4.9 for SAC405, which falls in region III, and 1.5 for Sn–Pb, which lies in region II.

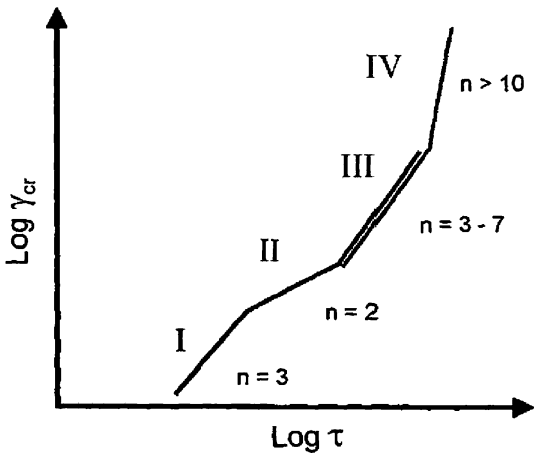

Fig. 23 Steady-state shear creep rate versus applied shear stress [16, 17]

Mechanisms of creep in lead-free solder alloys

Many mechanisms have been proposed for creep deformation for solder alloys, as the creep deformation map shows in Fig. 24, at higher stress levels the creep deformation is likely to involve dislocation glide and climb, while grain boundary diffusion (Coble Creep) and lattice diffusion (Nabarro-Herring Creep) may be the dominate creep mechanism at lower stress levels. Solder alloys are unique among other metals due to their extremely high homologous temperatures greater than $0.5T_m$ in their typical operating range. At higher stresses, it is believed that dislocation creep is the dominate creep mechanism in solders, involving the dislocation climb and moving away from barriers. At lower stresses, the lattice diffusion is believed to be the dominate mechanism for solder alloys, involving the diffusion and migration of interstitial atoms and lattice vacancies along the grain boundaries due to the applied tension stresses. Grain boundary sliding can be accompanied with the above mechanisms at any stress level.

Dutta et al. proposed a so-called glide-climb mechanism at lower stress regime and particle-limited climb at high stresses for lead-free solders [19], arguing that creep is induced by dislocation glide and climb at lower stress levels. The second phase particles (Ag_3Sn and Cu_6Sn_5) act to pin down the dislocations, preventing them from contributing to deformation via climb at lower stresses. When stresses are high enough for the dislocation to break the

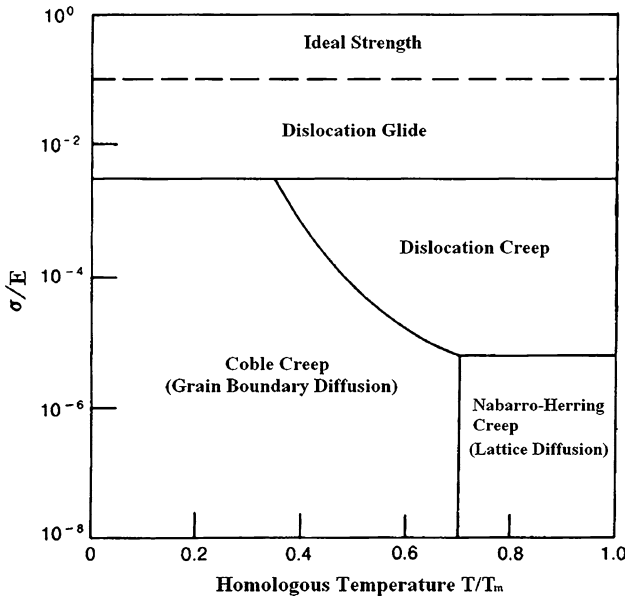

Fig. 24 A typical creep deformation map [2, 3]

threshold stress, the previously stuck dislocations will move rapidly to cause creep deformation, so the creep rate will increase rapidly after the applied stresses exceed the threshold stress needed for dislocations to break through.

Grivas et al. [18] suggested that the creep of Sn–Pb eutectic solder alloys exhibits both superplastic deformation and matrix creep. Superplasticity occurs at high temperatures ($>0.5T_m$), where the material exhibits great ductility before failure. The total strain can reach 1000% [1]. The dominant superplasticity mechanism is grain boundary sliding. For Sn–Pb, especially at elevated temperatures and low-stress levels, the creep mechanism will be a combination of superplastic and matrix creep, involving both dislocation creep and lattice diffusion creep.

Conclusions

SAC405 solder was found to have a higher creep resistance than Sn–Pb solder at the same stress level and testing temperature. The constitutive models obtained showed that the activation energy for SAC405 is much higher than that of Sn–Pb, which also indicates that SAC405 possesses higher creep resistance. This higher creep resistance is contributed by the second phase intermetallic compounds, Ag_3Sn and Cu_6Sn_5, which can effectively block dislocation movement and increase the creep resistance of the material.

Constitutive models of creep for both lead-free and Sn–Pb eutectic solders were constructed based on the experimental data. The activation energy for SAC405 is much higher than that of Sn–Pb, which also indicates that SAC405 possesses higher creep resistance. The constitutive models can be used in finite element analysis of actual electronic packages to predict solder joint failure. The creep mechanisms of both lead-free and Sn–Pb eutectic solders were also extensively discussed. Dislocation gliding and climb is believed to be the major failure mode at high stresses, while lattice diffusion and grain boundary diffusion is believed to be the major failure mode at low-stress levels. Grain boundary sliding is believed to contribute to creep deformation at both high-stresses and low-stresses. At lower stresses and high temperature, the superplastic deformation due to grain boundaries sliding is also believed to be a major creep mechanism for Sn–Pb.

References

1. Garofalo F (1966) Fundamentals of creep and creep-rupture in metals. The Macmillan Company, USA
2. Hertzberg RW (1996) Deformation and fracture mechanics of engineering materials, 4th edn. John Wiley & Sons Inc, NY
3. Evans RW, Wilshire B (1985) Creep of metals and alloys. The Institute of Metals, London
4. Mukherjee AK, Bird JE, Dorn JE (1969) Trans Am Soc Met 62:155
5. Clech JP. Review and analysis of lead-free materials properties, NIST, Available at: http://www.metallurgy.nist.gov/solder/clech/Sn-Ag-Cu_Main.htm
6. Ma H, Suhling JC, Lall P, Bozack M (2006) Reliability of the aging lead-free solder joints. In: Proceeding of the 56th electronic components and technology conference (ECTC), San Diego, California, May 30–June 2, 2006, pp 849–864
7. Ma H, Suhling JC, Lall P, Bozack M (2007) The influence of elevated temperature aging on reliability of lead-free solder joints. In: The proceeding of the 57th electronic components and technology conference (ECTC), May 2007, pp 653–668
8. Mitlin D, Raeder CH, Messler RW (1999) Metall Mater Trans A 30:115
9. Raeder CH, Mitlin D, Messler RW (1998) J Mater Sci 33(18): 4503. doi:10.1023/A:1004439931547
10. El-Rehim AFA (2008) J Mater Sci 43(4):1444. doi:10.1007/s10853-007-2312-4
11. Cheng F, Nishikawa H, Takemoto T (2008) J Mater Sci 43(10):3643. doi:10.1007/s10853-008-2580-7
12. Lau JH, Pang JHL, Ning-Cheng Lee, Luhua Xu (2007) Material properties and intermetallic compounds of Sn 3 wt% Ag 0.5 wt% Cu 0.019 wt% Ce (SACC). In: The proceedings of 57th electronic components and technology conference (ECTC07), pp 211–218
13. Tan KE, Xu L, Pang JHL (2008) Creep properties of Sn3 wt%AgO.5 wt%CuO.Ol9 wt%Ce (SACC) lead-free solder. In: The proceeding of 58th electronics packaging technology conference (ECTC08), pp 521–526
14. Dorn JE (1957) Creep and recovery. ASM Publication, Metal Park, OH, p 255
15. Weertman J (1968) ASM Trans Q 61:681
16. Hanke PL, Sprecher AF, Conrad H (1997) J Elec Materi 26:774
17. Schubert A, Walter H, Dudek R, Michel B, Lefranc G, Otto J, Mitic G (2001) Thermo-mechanical properties and creep deformation of lead-containing and lead-free solders. In: International symposium on advanced packaging materials, pp 129–134
18. Grivas D, Murty KL, Morris J, Jr (1979) Acta Metall 27:731
19. Dutta I, Park C, Choi S (2004) Mater Sci Eng A 379(40):1
20. Darveaux R, Banerji K (1992) IEEE Trans Compon Hybrids Manuf Technol 15(6):1013
21. Xiao Q, Armstrong WD (2005) J Elec Materi 34(2):196
22. Wiese S, Schubert A, Walter H, Dudek R, Feustel F, Meusel E, Michel B. Constitutive behavior of lead-free solders vs. lead-containing solders—experiments on bulk specimens and flip-chip joints. In: Proceeding of the 51st electronic components and technology conference, pp 890–902
23. Shi XQ, Wang ZP, Yang QJ, Pang HLJ (2003) J Eng Mater Technol 125:81
24. Zhang Q, Dasgupta A, Haswell P (2003) Viscoplastic constitutive properties and energy-partitioning model of lead-free Sn3.9Ag0.6Cu solder alloy. In: Proceeding of the 53rd electronic components and technology conference, pp 1862–1868
25. Darveaux R, Banerji K, Dody G (1995) Reliability of plastic ball grid array assembly. In: Lau JL (ed) Ball grid array technology. McGraw-Hill, New York, p 379
26. Vianco PT (2006) In: Shangguan D (ed) Fatigue and creep of lead-free solder alloys: fundamental properties. ASM International, pp 67–106
27. Lau J, Dauksher W, Vianco P (2003) Acceleration models constitutive equations reliability of lead-free solders and joints. In: Proceeding of the 53rd electronic components and technology conference, pp 229–236

28. Vianco PT, Rejent JA (2002) Compression deformation response of 95.5Sn-3.9Ag-0.6Cu Solder. UCLA Workshop on Pb-free Electronics. Available at: http://www.seas.ucla.edu/eThinFilm/PbfreeWorkshop/pdf/vianco.pdf
29. Pang JHL, Xiong BS, Low TH (2004) Creep and fatigue characterization of lead-free 95.5Sn-3.8Ag-0.7Cu solder. In: Proceeding of 54th electronic components and technology conference, pp 1333–1337
30. Schubert A, Dudek R, Auerswald E, Gollbardt A, Michel B, Reichl H (2003) Fatigue life models for SnAgCu and SnPb solder joints evaluated by experiments and simulation. In: Proceeding of the 53rd electronic components and technology conference, pp 603–610